

Supplementary Information

for

3D Printed Architected Conducting Polymer Hydrogels

Robert S. Jordan,^{1,†} Jacob Frye,^{1,†} Victor Hernandez,^{1,†} Isabel Prado,¹ Adrian Giglio,² Nastaran Abbasizadeh,³ Miguel Flores-Martinez,⁴ Kiana Shirzad,¹ Bohao Xu,¹ Ian Hill,¹ Yue Wang^{1,4,*}

¹ Department of Materials Science and Engineering, University of California, Merced, USA

² Department of Mechanical Engineering, University of California, Merced, USA

³ Quantitative and Systems Biology, University of California, Merced, USA

⁴ Department of Chemistry and Chemical Biology, University of California, Merced, USA

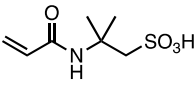
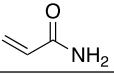
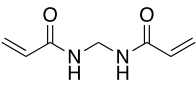
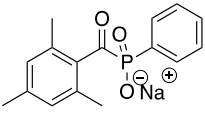
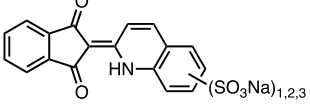
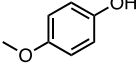
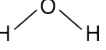
† Equal contribution

* Corresponding author

I. Precursor solution composition

The active ingredients in the precursor solution for the stereolithography (SLA) printing of PAMPSA-PAAm hydrogels are summarized below. Printing procedures are described in Experimental, and printer modifications are described in Section II of Supplementary Information.

Table S1. Active Precursors for the SLA Printing of PAMPSA-PAAm hydrogels.

Function	Chemical name	Chemical structure	Mass (g)	Molarity (mmol)
Monomers	2-Acrylamido-2-methyl-1-propanesulfonic acid * (AMPSA)		46.6	225.1
	Acrylamide ** (AAm)		5.4	75.97
Crosslinker	<i>N,N'</i> -Methylenebis (acrylamide) *** (MBAA)		1.9	12.32
Photoinitiator	Sodium phenyl(2,4,6-trimethylbenzoyl) phosphinate (Na-TPO)		3	9.67
Dye	Quinoline yellow ****		0.031	0.065
Inhibitor	4-Methoxyphenol (MeHQ) ***		0.068	0.548
Solvent	DI water		100	5549

Purchased from:

- * Sigma-Aldrich
- ** Fisher Scientific
- *** Alfa Aesar
- **** Acros Organics

II. SLA printer modification and printing mechanism

The construction of the Peopoly Moai printer is illustrated in Fig. S1a. In order to tailor the printing platform to our experimental needs, the following machine modifications were carried out.

Custom vat with reduced volume. The Moai came equipped with a 1-liter resin vat and a 169 cm² build plate, both too large for prototyping with custom precursor resins (Fig. S1b). To reduce the volume of precursor solution necessary for printing, we fabricated our own resin vats out of transparent acrylic sheets and tubing (Fig. S1c). The homebuilt vat consisted of a 2.778 mm (7/64 inch) thick acrylic sheet and a circular tube with outer diameter/inner diameter of 82.55/76.2 mm (3.25/3 inches), fused together using cyanoacrylate super glue. The acrylic sheet was cut down to the dimensions required to fit it securely into the guide rails of the SLA printer's tilt platform. Two narrow strips of the same 2.778 mm (7/64 inch) thick acrylic sheet were glued to the bottom of the vat where it interfaces with the guide rail to serve as spacers. Creating a gap between the vat and the tilt platform underneath prevented the vat bottom surface from being scratched, which could scatter the laser beam.

The custom vat utilized a hydrophobic polydimethylsiloxane (PDMS) film at the bottom of the vat interior to allow easy delamination of the growing print (Fig. S1d). The PDMS layer was replaced periodically as it fouls overtime with repeated laser exposure. The PDMS layer was prepared using the following procedure. In a clean plastic jar, 10 g of Part A and 1 g of Part B of the Cell Guard™ (ML Solar) PDMS precursors were mixed for 1 minute by hand using a plastic spatula. The PDMS mixture was then poured into the custom acrylic vat and left to degas and polymerize for ~24 hours followed by additional curing in a 50 °C oven for 2-3 hours.

Custom build plate. Due to the reduced size of the custom vat, the factory build plate could no longer fit into the vat. A smaller, hourglass-shaped build plate was designed and attached to the existing build plate as an extension. A borosilicate glass disk (diameter of 50.8 mm, thickness of 3.175 mm; Chemglass) was attached to this extension and used as the printing surface (Fig. S1c). The hourglass-shaped extension was 3D printed with a Formlabs Form 2 printer using their Clear Resin. The surface of the extension pointing towards the vat was covered by a layer of the yellow Lithoprotect® self-adhesive UV-protection foil. Heavy duty double-sided tape (3M 300lse) was used to adhere the hourglass extension to the original build plate and to adhere the borosilicate glass disk to the bottom of the extension covered with yellow foil. Finally, PTFE thread sealing tape was wrapped around the interface between the glass disc and the hourglass extension to prevent any resin from penetrating inside and delaminate the interface. The surface of the glass was thoroughly cleaned with water and air dried after each print.

Collectively, these customizations allowed the successful printing of conducting polymer hydrogels (Fig. S1e). Four lattice structures were fitted onto the built plate during each typical print.

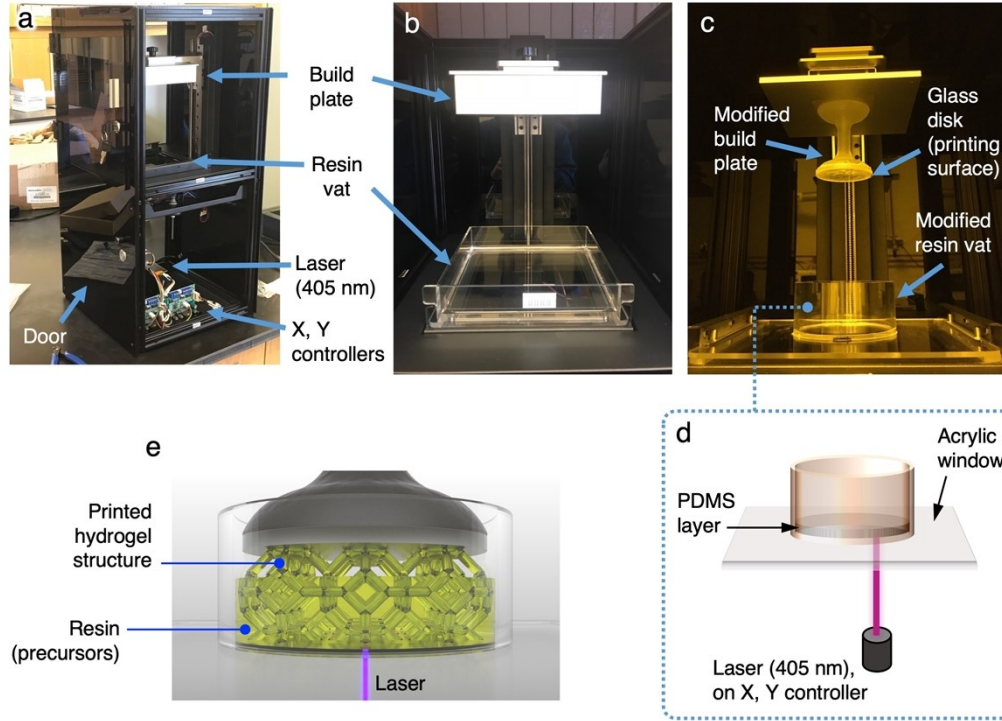


Figure S1. (a) Components within the Peopoly Moai stereolithography (SLA) printer. The build plate and resin vat area are enlarged in (b). (c) and (d) Photograph and schematic diagram, respectively, of the modified build plate and resin precursor vat.

III. Sodium TPO synthesis and characterization

Phenyl(2,4,6-trimethylbenzoyl)phosphinate (TPO) is considered one of the most efficient photoinitiators for UV-based 3D printing due to its high molar attenuation coefficient within the 365-405 nm range.¹ Unfortunately, it is not water soluble. Commercially available water-soluble photoinitiators such as Irgacure 2959 is not nearly as efficient as TPO, which requires longer exposure time for initiating photopolymerization.² We synthesized a water-soluble, ionic version of TPO through the reaction shown in Fig. S2a. The synthetic procedure is described in Experimental. Fig. S2b shows the ¹H NMR spectrum and peak assignment of the water-soluble sodium TPO, confirming its chemical identity.

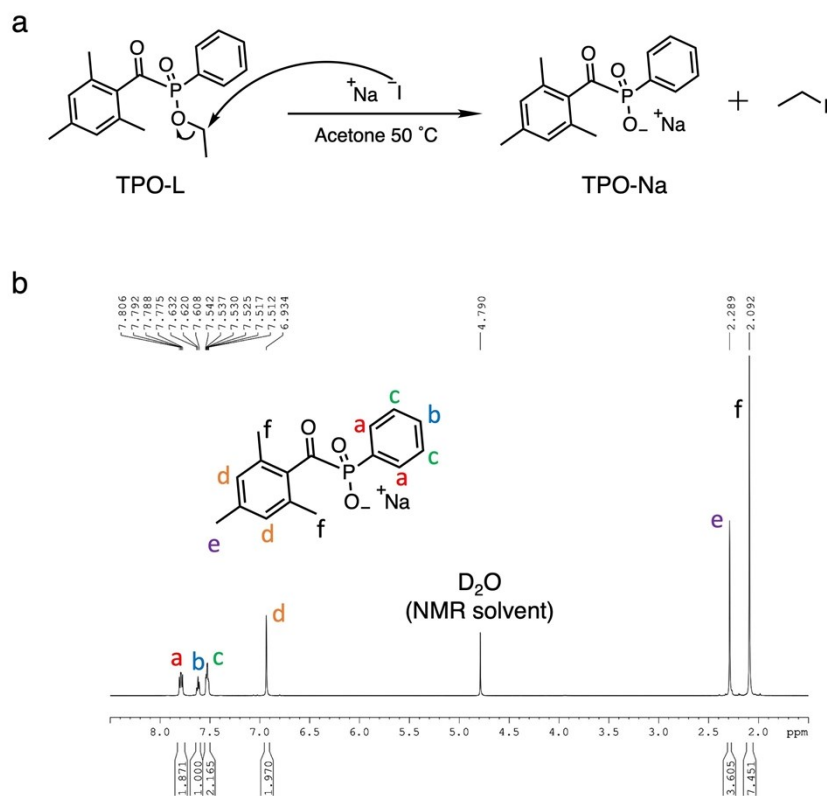


Figure S2. (a) Chemical reaction for the synthesis of sodium TPO (Na-TPO). (b) ¹H NMR spectrum of Na-TPO. Deuterated water was used as solvent. Peak assignments are labeled on the spectrum.

IV. Printing parameter optimization for hydrogel lattices

Here are the comprehensive set of data for the printing parameter optimization discussed in the main text.

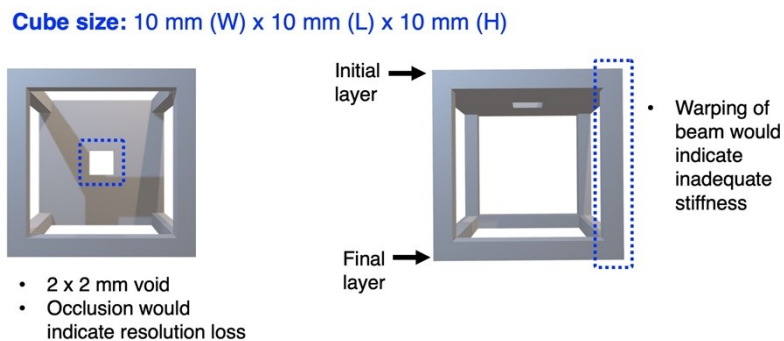


Figure S3. Rationale behind the structure designed for optimizing the printing parameters of complex 3D architected lattices.

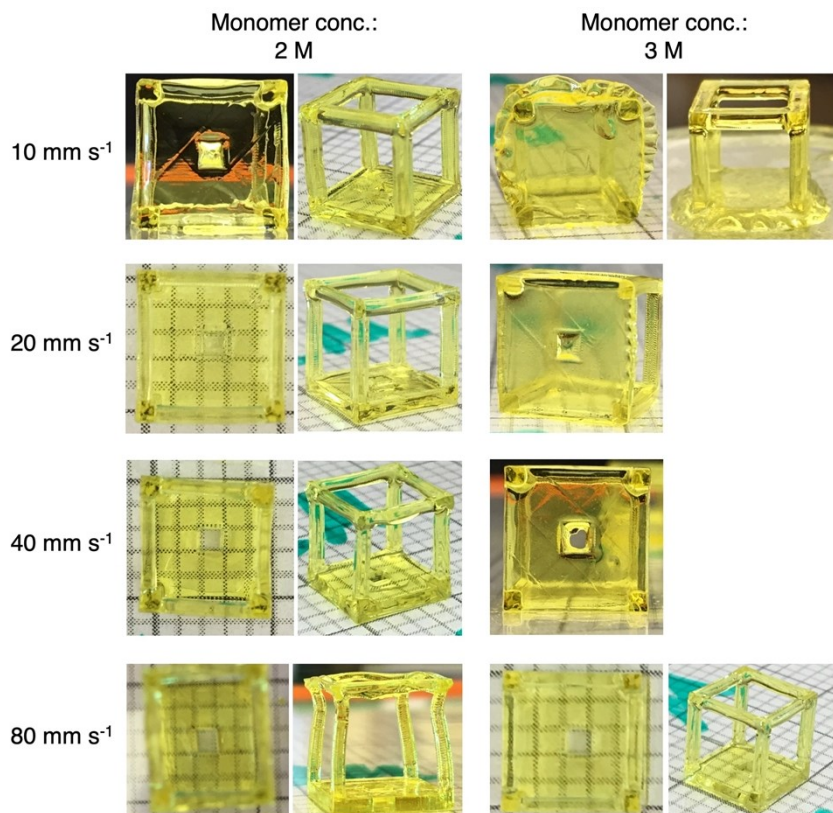


Figure S4. Photographs of the structure (CAD shown in Fig. S3) printed using different combinations of monomer concentration and laser speed.

V. Post-printing processing and PANI network synthesis

PANI network was grown in the 3D printed PAMPSA:PAAm hydrogel lattices. The transformation of the hydrogels through each step is shown in Fig. S5. For PANI growth, we found that pure aqueous growth conditions produced hydrogels with PANI only on the surface of hydrogels but not the interior. This is likely a result of the rapid growth of PANI at the hydrogel surface, forming a solid film that effectively blocks diffusion of additional reagents into the hydrogel. The PANI network grown using an interfacial method (described in Experimental) appeared to be consistent throughout the entirety of the hydrogel, and was used in this work.

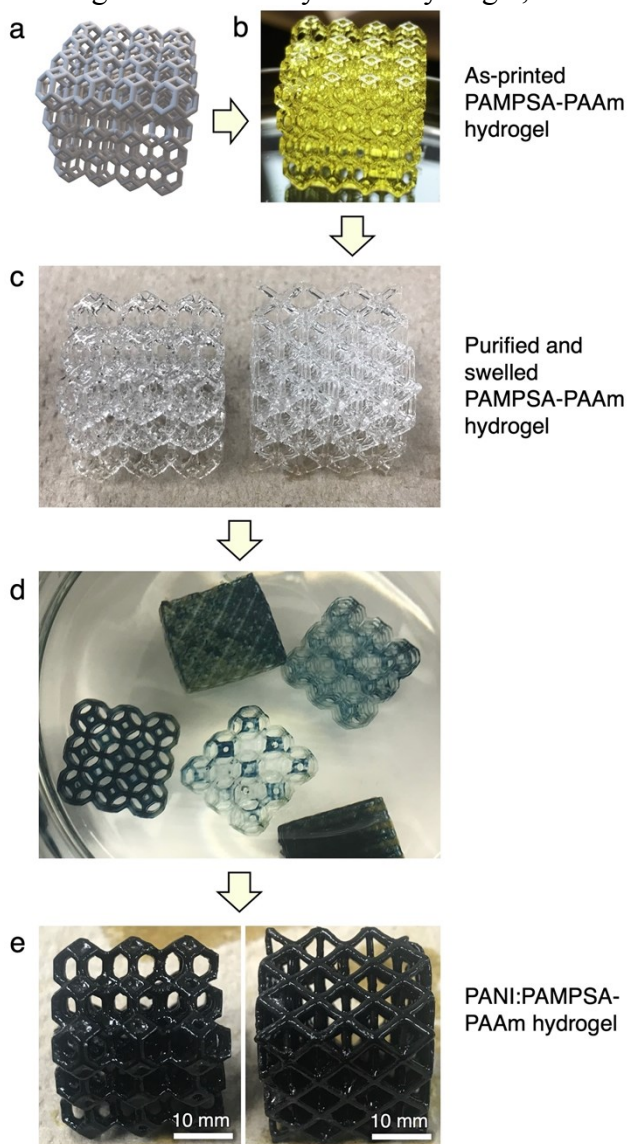


Figure S5. Photographic series showing the printing and processing of PANI hydrogel lattices. (a) and (b) CAD drawing and as-printed PAMPSA-PAAm hydrogel with a Kelvin lattice, respectively. (c) PAMPSA-PAAm hydrogel lattices after the removal of dye and other small molecule impurities by soaking in copious amount of deionized water. (d) Hydrogels during various stages of PANI (green in color) polymerization. (e) Purified PANI: PAMPSA-PAAm hydrogels.

VI. Chemical characterization

To confirm the growth of PANI in the hydrogel lattices, we carried out UV-vis-NIR and ATR-IR characterization.

UV-vis-NIR. PANI:PAMPSA-PAAm and the reference PAMPSA-PAAm samples for the UV-vis-NIR experiments were prepared by blending Kelvin lattice hydrogels (14% relative density) with 200 mL of deionized water using a Hamilton hand blender (Model 59762) at its lowest power setting for 5 sec. The homogenized dispersion was transferred to a 4 mL quartz vial for UV-vis-NIR measurements. The reference HCl-doped PANI sample was prepared by the following procedure adapted from literature.³ Aniline (0.3 g) was first dissolved in 10 mL of 1 M HCl. The aniline solution was then rapidly mixed with the oxidant solution containing 0.18 g of ammonium persulfate in 10 mL of 1 M HCl. The mixture was vigorously shaken for 15 seconds and left undisturbed overnight. The crude product was purified by three centrifugation cycles at 3,000 rpm for 15 minutes. After each centrifugation, the supernatant was decanted. The precipitant was redispersed in 40 mL of deionized water and centrifuged again. The final dispersion was diluted to a suitable concentration for UV-vis-NIR and the pH was adjusted to resemble the pH of the equilibrated PANI:PAMPSA-PAAm hydrogel (pH \approx 5-6).

The transparent PAMPSA-PAAm hydrogel does not absorb beyond \sim 250 nm (Fig. S6a). Three distinct peaks were observed for both the PANI:PAMPSA-PAAm hydrogel and PANI reference (Fig. S6a). The peaks at 294 nm for PANI:PAMPSA-PAAm and at 347 nm for PANI reference corresponds to the $\pi \rightarrow \pi^*$ transition in PANI.⁴ The blue shift of the $\pi \rightarrow \pi^*$ transition in the PANI:PAMPSA-PAAm hydrogel sample compared to the reference suggests the molecular weight of PANI in the hydrogel is likely lower than that of PANI synthesized via conventional chemical polymerization.⁴ This reduced molecular weight could be the result of the limited diffusion of aniline monomers into the hydrogel lattice. Both PANI:PAMPSA-PAAm hydrogel and the PANI reference sample exhibit absorptions at around 420 and 790 nm, which can be ascribed to the polaron band $\rightarrow \pi^*$ and $\pi \rightarrow$ polaron band transitions, respectively.⁴ These characteristic peaks confirm the presence of PANI and that it is in the doped, emeraldine salt oxidation state.

ATR-IR. The ATR-IR samples for the hydrogels were prepared by drying the hydrogels at 60 °C overnight in a convection oven. The dried structure was then crushed into a powder using mortar and pestle for ATR-IR measurements.

In order to distinguish the peaks attributed to PANI versus PAMPSA:PAAm in the PANI:PAMPSA-PAAm hydrogels, the control sample of HCl-doped PANI synthesized for the UV-vis-NIR experiment was dried at 60 °C overnight. The solid pellet was removed from the centrifuge tube and directly used for ATR-IR data collection as the reference spectra for PANI.

The ATR-IR spectra of dried PANI:PAMPSA-PAAm contains features of both PANI and PAMPSA-PAAm, confirming that PANI was successfully grown (Fig. S6b). Two peaks associated with PAMPSA-PAA that are shared by the two hydrogel samples, appear at 1643 cm^{-1} , corresponding to the C=O stretch of the amide of the crosslinked PAMPSA-PAAm backbone and at 1031 cm^{-1} , which can be attributed to $-\text{SO}_3\text{H}$ vibration from PAMPSA side groups.⁵ In contrast,

the PANI:PAMPSA-PAAm gel spectra has a stronger signal in the 790 cm^{-1} region which is ascribed to the out-of-plane C-H vibration of PANI, and a peak around 1113 cm^{-1} attributed to in-plane bending of C-H in aromatic moieties.⁶ The PANI spectrum displays the quinonoid and benzenoid structures at around 1563 and 1482 cm^{-1} , respectively.⁵ These peaks are not distinct in the PANI:PAMPSA-PAA spectrum as they overlap with peaks associated with PAMPSA-PAAm at 1541 and 1643 cm^{-1} . The 1643 cm^{-1} peak in the PANI:PAMPSA-PAA spectrum is highly asymmetrical, with the baseline higher to the right side of those peaks. This indicates that the peak is comprised of multiple peaks, likely containing the 1563 cm^{-1} PANI peak. The 1482 cm^{-1} peak is also buried in the PANI:PAMPSA-PAA spectrum likely for similar reasons.

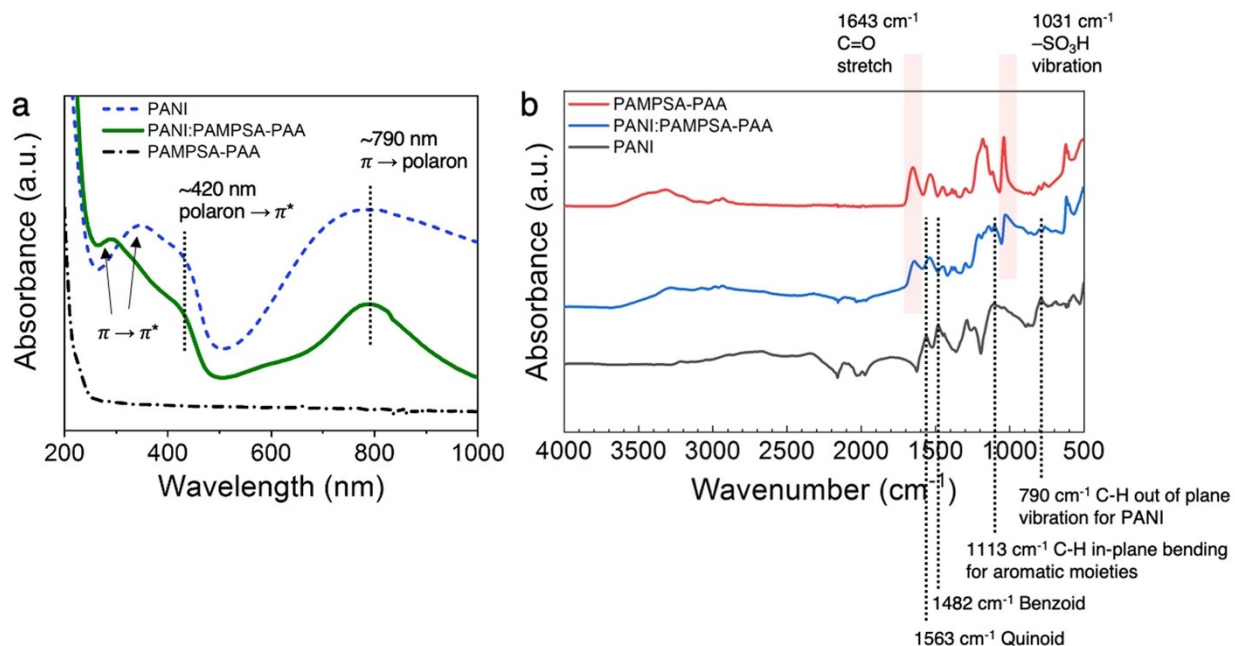


Figure S6. Chemical characterization of the 3D printed hydrogels confirming the presence of PANI in its doped, emeraldine salt oxidation state. (a) UV-vis-NIR and (b) ATR-IR spectra for the PANI:PAMPSA-PAA hydrogel compared to PAMPSA-PAAm and PANI references. Peak assignments are labeled on the spectra.

VII. Relative density calculation

The relative density of a lattice material is defined as the ratio of the density of porous lattice to the density of the solid. The theoretical volumes of the lattices were calculated using the volume calculation command in Rhinoceros 3D. Volumes were adjusted to the desired amount by changing the radius of the beam elements. The unit cells for each lattice type had equal external dimensions. Any changes in the external size of the lattice retained the volume ratio, as it was equally scaled in all directions.

Accurately measuring the relative densities of the hydrated hydrogels is challenging due to the various amount of water trapped in the void space within the lattices. Through a series of control experiments using solid hydrogels, we found that the hydrated and dried structures have identical relative density when hydrogels were dried isotropically. Therefore, we calculated the relative density for each hydrogel lattice from their dehydrated state. Isotropic drying was achieved by placing the hydrogels (solid or architected lattices) on a weaved Teflon sheet and let the water slowly evaporate under ambient conditions. The weaved texture provided pores for water evaporation from the bottom of the hydrogel in addition to the exposed surfaces, and the low friction, hydrophobic Teflon surface prevents any interfacial pinning during dehydration.

VIII. Supplementary mechanical characterization data

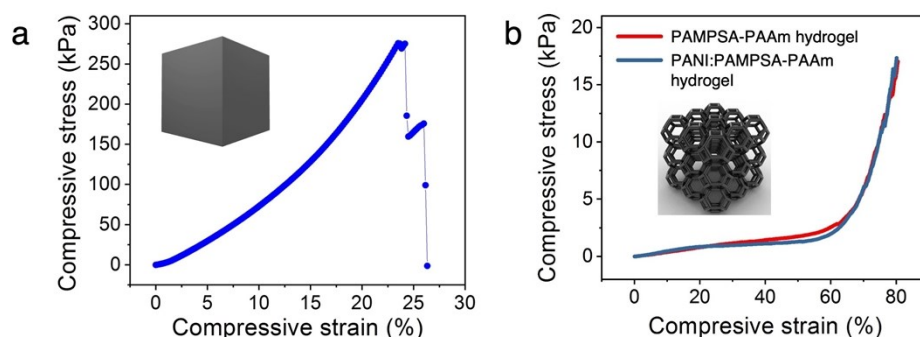


Figure S7. (a) Stress-strain curve for a printed solid cube of PANI:PAMPSA-PAAm hydrogel. The printing and post-processing procedures used for the solids are identical to those used for the architected lattices. (b) Stress-strain behavior of the 14% relative density PANI:PAMPSA-PAAm Kelvin lattice hydrogel compared to the same hydrogel lattice prior to PANI growth. The two curves closely overlap, indicating the PAMPSA-PAAm dopant network provides the mechanical properties of the lattice. However, the PANI:PAMPSA-PAAm hydrogel exhibited a slightly lower stress in part of the plateau region, possibly due to the slightly lower water content in these PANI-containing hydrogels (~98 wt%) compared to the PAMPSA-PAAm hydrogels (~99 wt%). This minor difference is likely caused by the more hydrophobic nature of PANI compared to PAMPSA.

IX. *In-situ* resistance-stress-strain measurement setup

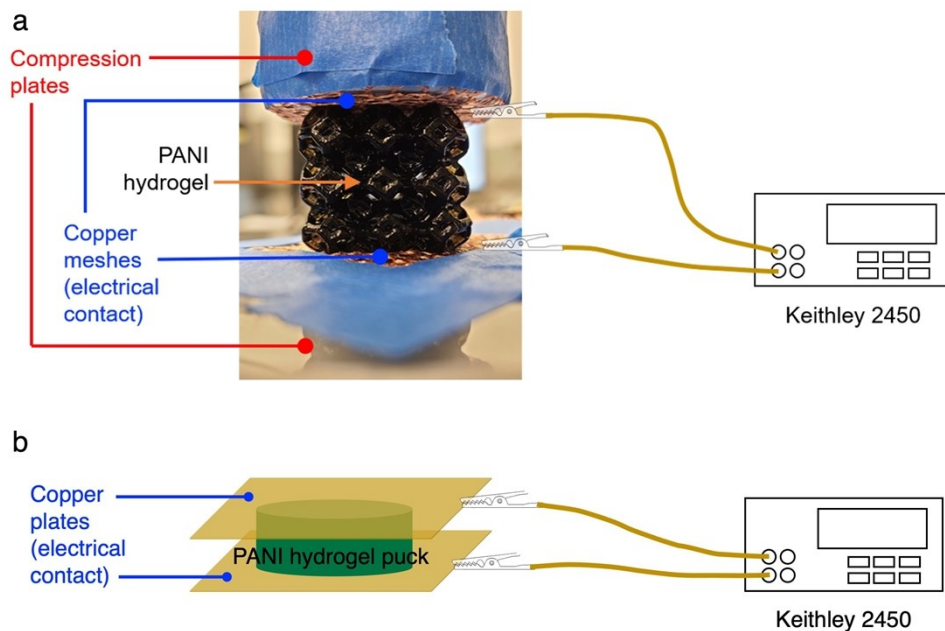


Figure S8. (a) Schematic diagram of the *in-situ* electrical-mechanical characterization of architected PANI hydrogel lattices. The copper meshes are affixed on the compression plates. Copper meshes were selected as electrodes as the mesh structure provides adequate friction to prevent hydrogels from slipping out. Fresh copper meshes were used for each measurement. (b) Schematic diagram showing the geometry for conductivity measurements.

References

1. M. G. Neumann, W. G. Miranda, C. C. Schmitt, F. A. Rueggeberg and I. C. Correa, *J. Dent.*, 2005, **33**, 525–532.
2. B. Zhang, S. Li, H. Hingorani, A. Serjouei, L. Larush, A. A. Pawar, W. H. Goh, A. H. Sakhaei, M. Hashimoto, K. Kowsari, S. Magdassi and Q. Ge, *J. Mater. Chem. B*, 2018, **6**, 3246–3253.
3. Z. D. Zujovic, Y. Wang, G. A. Bowmaker and R. B. Kaner, *Macromolecules*, 2011, **44**, 2735–2742.
4. Y. Wang, H. D. Tran, L. Liao, X. Duan and R. B. Kaner, *J. Am. Chem. Soc.*, 2010, **132**, 10365–10373.
5. J.-W. Jeon, Y. Ma, J. F. Mike, L. Shao, P. B. Balbuena and J. L. Lutkenhaus, *Phys. Chem. Chem. Phys.*, 2013, **15**, 9654.
6. Y. Wu, Y. X. Chen, J. Yan, S. Yang, P. Dong and P. Soman, *J. Mater. Chem. B*, 2015, **3**, 5352–5360.